





REPORT

 OPEN ACCESS



Modulation of protein A binding allows single-step purification of mouse bispecific antibodies that retain FcRn binding

Adam Zwolak ^{a,†}, Anthony A. Armstrong^{a,†}, Susan H. Tam ^a, Jose R. Pardinás^a, Dennis R. Goulet ^b, Songmao Zheng^c, Kerry Brosnan^d, Eva Emmell^d, Jeffrey Luo^a, Gary L. Gilliland ^a, and Mark L. Chiu^a

^aBiologics Discovery, Janssen Research & Development, LLC, Spring House, PA, USA; ^bDepartment of Medicinal Chemistry, University of Washington, Seattle, WA, USA; ^cBiologics Development Sciences, Janssen Research & Development, LLC, Spring House, PA, USA; ^dBiologics Toxicology, Janssen Research & Development, LLC, Spring House, PA, USA

ABSTRACT

The increased number of bispecific antibodies (BsAb) under therapeutic development has resulted in a need for mouse surrogate BsAbs. Here, we describe a one-step method for generating highly pure mouse BsAbs suitable for *in vitro* and *in vivo* studies. We identify two mutations in the mouse IgG2a and IgG2b Fc region: one that eliminates protein A binding and one that enhances protein A binding by 8-fold. We show that BsAbs harboring these mutations can be purified from the residual parental monoclonal antibodies in one step using protein A affinity chromatography. The structural basis for the effects of these mutations was analyzed by X-ray crystallography. While the mutation that disrupted protein A binding also inhibited FcRn interaction, a bispecific mutant in which one subunit retained the ability to bind protein A could still interact with FcRn. Pharmacokinetic analysis of the serum half-lives of the mutants showed that the mutant BsAb had a serum half-life comparable to a wild-type Ab. The results describe a rapid method for generating panels of mouse BsAbs that could be used in mouse studies.

ARTICLE HISTORY

Received 2 March 2017
Revised 30 August 2017
Accepted 30 August 2017

KEYWORDS

antibody; bispecific; x-ray crystallography; calorimetry; pharmacokinetics

Introduction

Therapeutic biologics programs are increasingly turning to bispecific antibodies (BsAbs), which are Abs containing two distinct antigen binding (Fab) regions. Indeed, many such bispecific therapeutics for dual-antigen targeting, cell redirection efforts, and immune checkpoint modulation are currently in clinical trials,^{1–3} although high-throughput production of highly pure BsAbs presents challenges. The development of human IgG-based BsAbs to be generated on a manufacturing scale was initially limited by the difficulty of separating the desired BsAb from undesired antibody species that could be present in production mixtures.⁴ For example, BsAb can be generated by co-transfection of two heavy chains (HC) and two light chains (LC), resulting in a small amount (< 10%) of desired BsAb among a majority of contaminating species, but this approach is not feasible for large-scale or high-throughput efforts. Although novel F_v-based molecules and non-IgG based scaffolds can alleviate HC-HC and HC-LC pairing issues,⁵ IgG-based bispecific molecules are often attractive on the basis of their longer serum half-lives, lower likelihood of having anti-drug responses, and their amenability to engineering to modulate Fc effector functions such as antibody-dependent cell-mediated cytotoxicity (ADCC) or antibody-dependent cellular phagocytosis (ADCP).

Thus, substantial effort has been put into optimizing pairing between HC-HC and between HC-LC. To generate BsAbs, the HC molecules require heterodimerization while the LC molecules must pair with the correct cognate HC. Some examples of successful strategies to influence HC-HC pairing include knobs-into-holes (KIH),⁶ electrostatic steering,⁷ and controlled Fab arm exchange (cFAE).^{8–10} These methods all involve introduction of complementary mutations into the C_{H3} domain to favor formation of heterodimerization of Fc regions. To generate BsAb by co-transfection of HC plasmids requires additional methods to ensure correct HC-LC pairing.^{4,11,12} The cFAE method ensures proper HC-LC pairing by using separately expressed and purified parental mAbs containing the complementary HC mutations F405L or K409R. The parental mAbs that are mixed and incubated under mild reducing conditions and subsequent oxidation. The reaction generally results in greater than 90% heterodimer formation of human IgG1 BsAb,⁸ and was later shown to be effective when separately expressed mAbs are subjected to cFAE directly from culture supernatants.¹³

To better validate the therapeutic efficacy of IgG biologics, drug discovery programs frequently use mouse IgG Abs as surrogates for *in vivo* studies, particularly mouse IgG2a and mouse IgG2b since they display greater Fcγ receptor-

CONTACT Adam Zwolak  azwolak@its.jnj.com  Biologics Discovery, Janssen Research & Development, LLC, 1400 McKean Road, Spring House, PA 19477, USA; Mark L. Chiu  mchiu@its.jnj.com  Biologics Discovery, Janssen Research & Development, LLC, 200 Great Valley Parkway, Malvern, PA 19355, USA.

 Supplemental data for this article can be accessed on the [publisher's website](#).

[†]equal contribution

© 2017 Janssen Research and Development. Published with license by Taylor & Francis Group, LLC

This is an Open Access article distributed under the terms of the Creative Commons Attribution-NonCommercial-NoDerivatives License (<http://creativecommons.org/licenses/by-nc-nd/4.0/>), which permits non-commercial re-use, distribution, and reproduction in any medium, provided the original work is properly cited, and is not altered, transformed, or built upon in any way.

mediated effector function compared with mouse IgG1 and mouse IgG3 Abs.¹⁴ Mouse IgG2a and IgG2b Abs can be generated by cFAE, although efficient BsAb formation requires two additional mutations (T/V370K, F405L and K409R, R411T) to favor HC pairing.¹⁵ Mouse BsAbs have also been generated by other methods, including KIH technology.^{16,17} While these methods can lead to relatively efficient BsAb formation, removal of contaminating parental mAb and Ab fragments is still required, especially in cases where parental Ab can have a confounding effect on experimental results. Additionally, in cases where parental mAbs are co-transfected, expression levels of each polypeptide chain results in significant populations of undesired contaminating species. Removal of these species, which can have similar biophysical characteristics as the desired BsAb, can be time consuming. Thus, methods for high-throughput purification of mouse BsAb heterodimers are of critical importance.

Large scale and high-throughput purification of bispecific IgG molecules requires robust, preferably single-step purification methods that use commercially available resins, such as those based on staphylococcal protein A. Stability-enhancing mutations introduced into a domain of protein A led to a synthetic fragment termed the Z-domain.¹⁸ Tandem Z-domains have been engineered into commercial Fc affinity resins that are resistant to high pH treatment and which bind only the Fc region.^{19,20} Abs are purified using Z-domain affinity resin by binding at neutral pH and eluting in acidic pH buffer. The pH value at which IgG can be eluted from protein A resin depends on its affinity for protein A. In fact, differences in affinities for protein A have been observed between IgG isotypes, and these affinity differences result in different pH values at which they can be eluted from immobilized protein A.^{21,22}

Modulation of the protein A binding characteristics of Abs can significantly decrease serum half-life since both protein A and the neonatal Fc receptor (FcRn) share a binding site on the Fc.²³ FcRn is largely responsible for maintaining the long serum half-life of IgG²⁴⁻²⁹ via its ability to bind with high affinity to IgG at acidic pH (< 6.5) in the recycling endosome and to dissociate at neutral pH, releasing the IgG back into the serum and thus saving IgG from lysosomal degradation.^{30,31} For example, mutation of isoleucine at position 253 (I253), which is conserved across human and mouse IgG molecules, to alanine almost entirely abolishes binding to FcRn.^{32,33}

We sought to develop a higher-throughput method to purify BsAb from contaminating parental mAbs and Ab fragments. We hypothesized that two different mouse IgG variants that bound Z-domain with different affinities could be separated by protein A-affinity chromatography at different pH values, allowing one-step generation of BsAb, analogous to a previous effort using human IgG1 Abs.³⁴ Here, we describe two sets of mutations in mouse IgG2a and IgG2b, one which abolished protein A binding and one which, remarkably, enhanced protein A binding. BsAbs in which each heavy chain harbored one of these mutations were separated from the residual parental mAbs by step elution from protein A resin at different pH values. We analyzed the effects of these mutation sets on Fc receptor interaction *in vitro* and on serum half-life *in vivo*. The

structural basis for the effects of these mutations was determined by X-ray crystallography. Combined, the results described a method for one-step purification of > 95% pure mouse BsAb having serum half-lives comparable to wild-type mouse Abs.

Results

Rationale for mutations and their effects on protein A binding

We measured the affinity of IgG molecules for protein A by isothermal titration calorimetry (ITC) using a previously described synthetic three-helix Z-domain derived from protein A (Supplementary Fig. 1a).¹⁸ As a control, the affinity (K_D) of human IgG1 for Z-domain was measured as 23 nM (Table 1, Supplementary Fig. 1b), which was similar to previously reported measurements.^{19,35-37} Mouse IgG2a and IgG2b bound Z-domain with weaker affinity, having K_D values of 0.2 and 3.6 μ M, respectively (Fig. 1a, Table 1, Supplementary Fig. 1c and d). Since mutation of the highly conserved I253 was known to disrupt protein A binding,^{32,33} we introduced I253D to generate a weak-binding parental Ab. Mutation of isoleucine 253 to aspartate (I253D) in mouse IgG2a or IgG2b abolished binding to Z-domain (Fig. 1a, Supplementary Fig. 1e). Because of the weaker binding of mouse IgG2a and IgG2b relative to human IgG1, we sought to identify mutations that would enhance binding to protein A, leading to a parental Ab that would elute only at low pH. IgG binds Z-domain using three loops in the Fc region, two from the C_H2 and one from C_H3 domain.³⁸ By sequence comparison of mouse and human IgG Fc regions, we identified P307 and Q309 in mouse IgG2a and IgG2b, which are conserved in mouse IgG2a, IgG2b, and IgG3 but differ in human IgG1, as potentially contributing to the difference in affinity (Supplementary Fig. 2a). Human IgG1, which binds Z-domain much more tightly, contains threonine 307 (T307) and leucine (L309), which contribute to high affinity protein A binding.

The mutations proline 307 to threonine (P307T) and glutamine 309 to leucine (Q309L) increased the affinity of mouse IgG2b for Z-domain by ~8-fold relative to wild-type mouse IgG2b and provided a modest affinity increase for mouse IgG2a (Fig. 1a, Supplementary Fig. 2b, Table 1). The difference in affinity of the mutants for Z-domain resulted in elution from immobilized protein A resin at a lower pH than a wild-type mouse Ab at the same ionic strength (Fig. 1b). We hypothesized that if the difference in elution pH for mouse Abs possessing the I253D or the P307T, Q309L mutations was large, then a mouse BsAb, wherein each heavy chain subunit harbored one of the mutation sets would elute at an intermediate pH value. Thus, the mouse BsAb could be purified from contaminating parental mouse mAbs using a pH step-gradient.

Purification of mutant bispecific antibodies

We tested whether differences in affinity would result in different pH values at which the mouse IgG2a and IgG2b variants could be eluted from protein A resin. Note that the affinity resin (mAbSelect SuRe, GE Healthcare), which comprised tandem Z-domain moieties, has a higher affinity for the Fc than

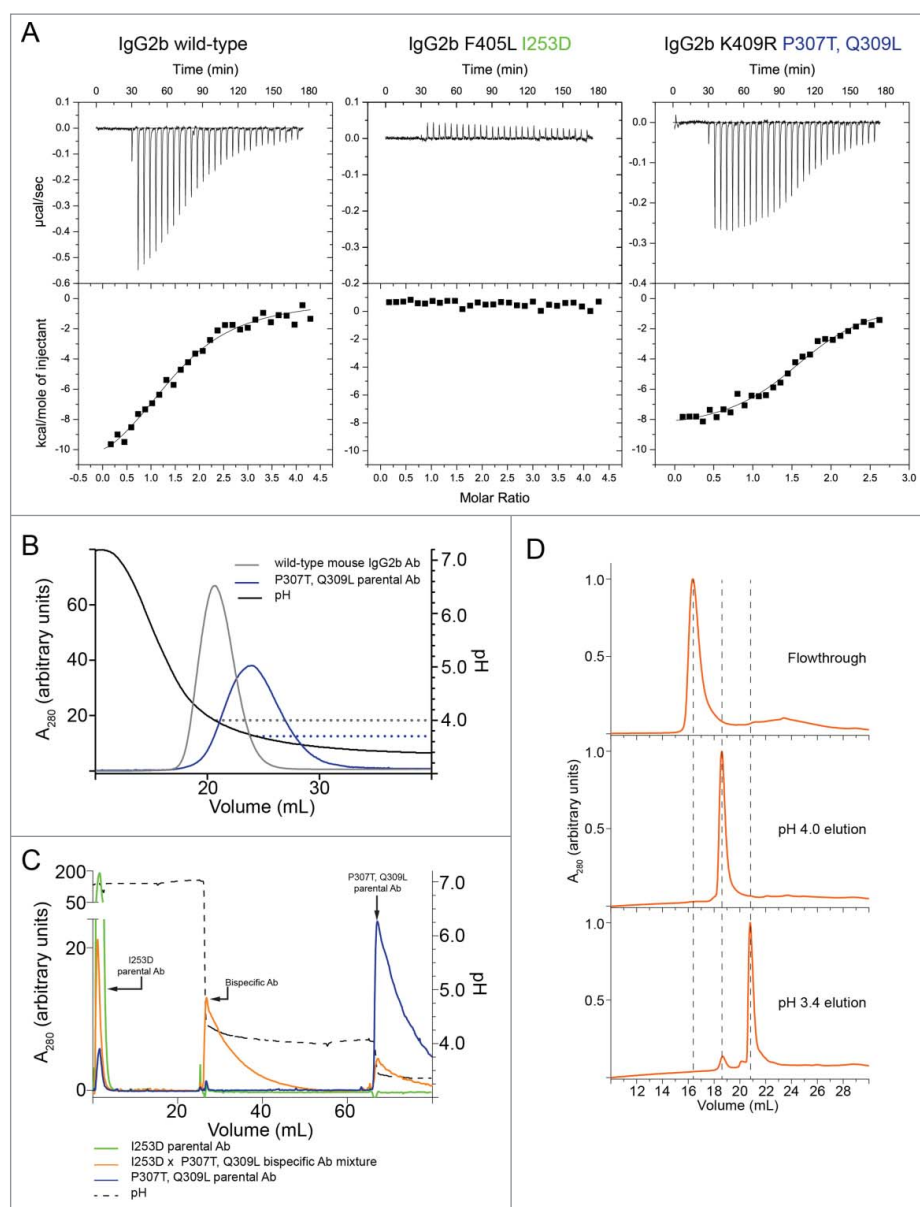


Figure 1. Binding of IgG2b to Z-domain and differential affinity purification. (A) Isotherms resulting from the binding of Z-domain to mouse IgG2b variants. Top panels show power input vs mole ratio of injectant (Z-domain) to titrant (IgG). Bottom panels plot the corresponding binding enthalpy. (B) Purification chromatograms of mouse IgG2b variants by 3-step pH gradient using mAbSelect Sure (GE Healthcare) affinity resin. The left y-axis shows absorbance at 280 nm and the right y-axis shows buffer pH vs elution volume. One mg each of mouse IgG2b was loaded in each experiment. (C) The elution fractions from each elution step: pH 7.2, 4.0, and 3.4 for the mixed sample containing both parental Abs and the bispecific Ab (orange trace in panel b) were analyzed by hydrophobic interaction chromatography (HIC). Dashed lines indicate the elution volume of the two parental mouse Abs and the mouse BsAb. Note that the elution volume of the mouse BsAb was intermediate between that of the parental mouse Abs.

Table 1. Binding constants and stoichiometry of Z-domain binding to IgG variants.

| Protein | K_D (μM) ^a | ΔH (kcal/mol) | $-T\Delta S$ (kcal/mol) | N^b |
|-----------------------------|--------------------------------------|-----------------------|-------------------------|-------|
| Human IgG1 | 0.02 ± 0.02 | -37.7 ± 23.2 | 27.1 ± 23.8 | 1.74 |
| Mouse IgG2a | 0.20 ± 0.03 | -15.2 ± 9.6 | 6.1 ± 1.0 | 1.52 |
| Mouse IgG2b | 3.65 ± 1.40 | -17.8 ± 8.5 | 10.3 ± 8.7 | 1.87 |
| Mouse IgG2b ^l | 2.60 | -4.2 | -3.35 | 1.23 |
| Mouse IgG2b I253D | No binding | | | |
| Mouse IgG2b P307T, Q309L | 0.47 ± 0.11 | -18.3 ± 6.4 | 9.7 ± 6.4 | 1.65 |
| Mouse IgG2b Fc P307T, Q309L | 0.39 | -9.4 | 7.23 | 1.24 |
| Mouse IgG2a I253D | No binding | | | |
| Mouse IgG2a P307T, Q309L | 0.13 ± 0.02 | -16.9 ± 6.5 | 7.5 ± 0.8 | 1.23 |

^aAverage \pm standard deviation of 2 or 3 independent measurements

^bBinding to Z34C peptide used in crystallographic studies

native protein A and does not bind the Fab region.²⁰ The binding between mouse IgG and Z-domain peptide was confirmed to be solely within the Fc since Z-domain bound to the Fc (containing the P307T, Q309L mutations) alone with an affinity similar to that of the full-length mouse mAb (Table 1, Supplementary Fig. 2c). Wild-type mouse IgG2b eluted at pH 4.4 from the resin (Fig. 1b). As expected, the mouse IgG2b I253D mutant did not bind the resin, and eluted in the flowthrough at pH 7.2, while the P307T, Q309L mutant eluted only at pH 3.4. The large difference in elution pH between the two mutants suggested that a mouse BsAb, with each heavy chain subunit harboring one of these two mutation sets, would elute at an

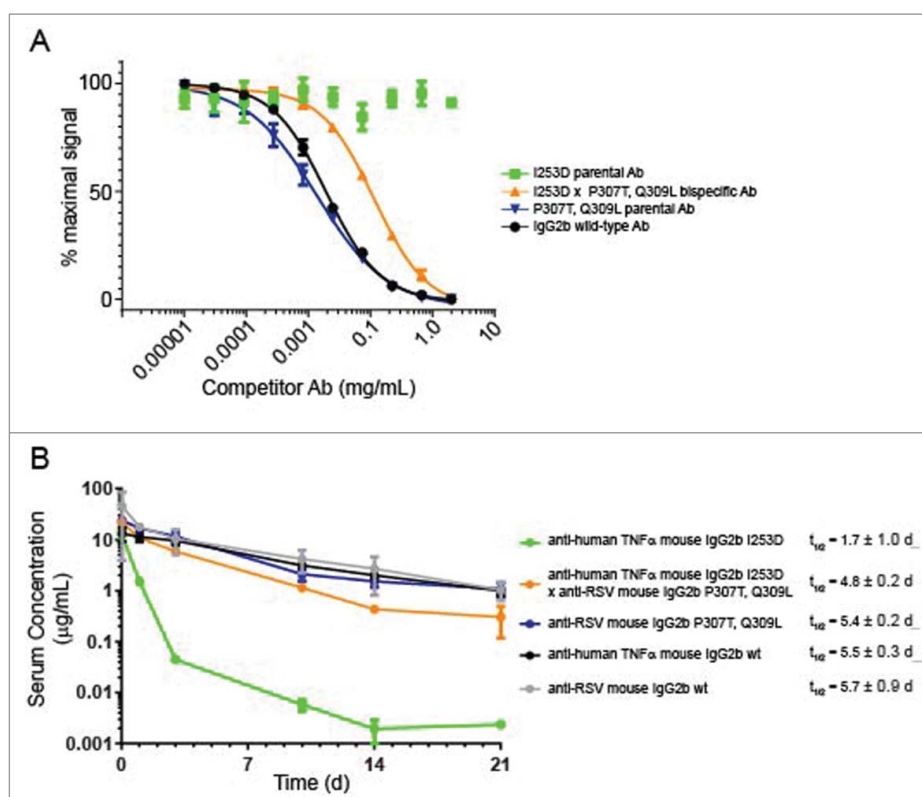


Figure 2. Analysis of FcRn interaction and PK analysis. (A) Competition binding of mouse IgG2b variants with wild-type IgG2b for FcRn using AlphaScreen assay. The graph displays % maximum signal plotted vs concentration of competitor. Mouse IgG2b wild-type compares the ability of the Ab to compete with itself as a control. (B) Pharmacokinetic analysis of mouse IgG2b variants in C57BL/6 mice. The graph displays the concentration of each Ab vs time after injection. Each point represented the mean \pm standard error of 6 animals per group. Antibody specificities are indicated on the plot.

intermediate pH, allowing its purification from the mutant parental mouse mAbs.

To test this hypothesis, we first prepared a mouse IgG2b BsAb using the cFAE method.⁸ To test whether the BsAb could be efficiently purified by differential protein A elution, the BsAb solution was mixed with the two parental mAbs at an equimolar ratio. This mixture of parental and bispecific mouse Abs were resolved by a multiple pH step elution (Fig. 1c). The composition of each elution step was analyzed by hydrophobic interaction chromatography (HIC), which showed that the I253D Abs could be separated from the P307T, Q309L Abs based on the different hydrophobicity of their Fab regions (Fig. 1d). The flowthrough was found to contain the I253D parental mAb, while the pH 4.0 eluent contained only BsAb, and the pH 3.4 eluent contained almost exclusively (> 95%) parental mAb harboring the P307T, Q309L mutation.

We introduced the mutations into a mouse IgG2a framework, and analyzed them in the same way. Mutation of T370K further improved yields of mouse BsAb during cFAE when combined with K409R, so this mutation was included for the mouse IgG2a studies (data not shown). As expected, mouse IgG2a harboring the I253D mutation did not bind Z-domain and thus flowed through the affinity column during a wash step (Supplementary Fig. 3a). Surprisingly, although mouse IgG2a P307T, Q309L bound Z-domain more tightly than the corresponding mouse IgG2b variant at pH 7.2 ($K_D \sim 126$ nM vs 468 nM), this mouse IgG2a variant eluted at higher pH values (4.4 vs 3.4). This was also true of the wild-type mouse molecules (Table 1). However,

the introduction of the P307T, Q309L mutations provided a modest improvement in affinity and decreased the elution pH of mouse IgG2a Abs, allowing these molecules to be eluted at lower pH values. An equimolar mixture of an I253D parental mouse mAb, a P307T, Q309L parental mouse mAb, and the resultant mouse BsAb ($\sim 33\%$ purity of each species), was separated using a 3-step pH gradient (pH 7.2, 4.9, and 3.4), allowing the mouse BsAb to be purified to $\sim 82\%$ purity (Supplementary Fig. 3), based on HIC analysis.

We also tested the purification of a muIgG2b BsAb formed in culture supernatants. A mixture of culture supernatants containing approximately equimolar amounts of parental mAbs with either I253D or P307T, Q309L mutations was prepared and subjected to in-supernatant cFAE as described.¹³ The mixture was then purified by protein A-affinity chromatography using a step gradient, and the fractions were analyzed by HIC (Supplementary Fig. 4). The intermediate pH elution contained > 95% pure mouse BsAb while the low pH elution (pH 3.4) contained < 3% residual BsAb, having $\sim 97\%$ P307T, Q309L parental Ab. This result showed that the differential protein A purification method was also amenable to purification from in-supernatant cFAE-derived material.

Analysis of Fc receptor interaction and serum half-life

To assay the extent to which the mutations affected FcRn binding, we used two *in vitro* methods. In an AlphaScreen competition-based assay (Perkin Elmer), the binding of a labeled

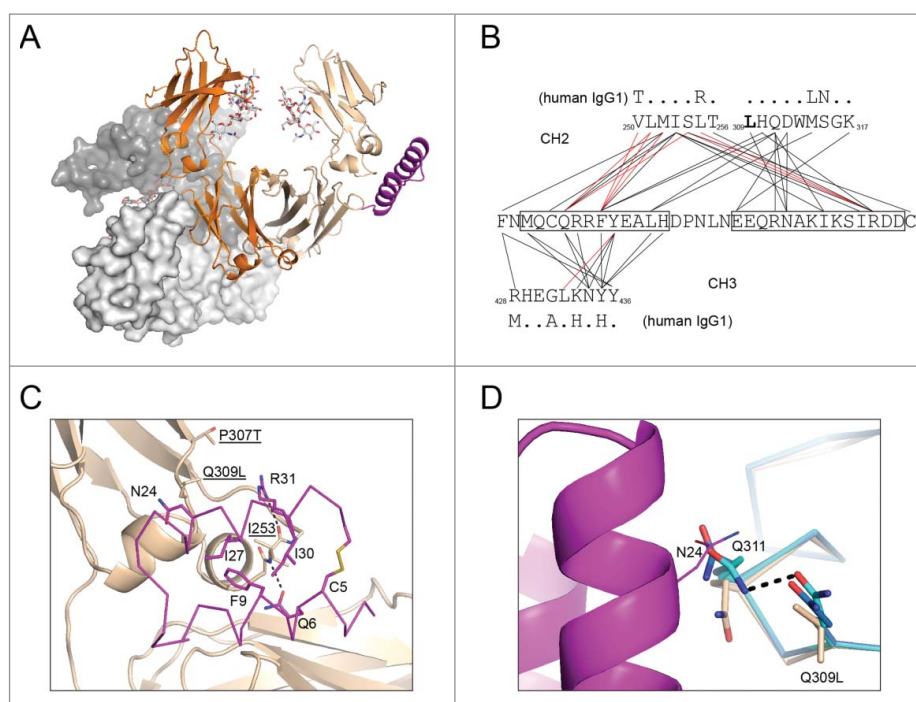


Figure 3. Structural basis of altered protein A binding by IgG2b variants. (A) Fc and Z34C are shown in cartoon with I253D-containing chain colored orange; P307T, Q309L-containing chain colored wheat; Z34C colored magenta. N297 linked glycans are shown in stick (light grey). The crystallographically related Fc dimer that blocks the equivalent Z34C binding site on the I235D chain is shown in light and dark grey surface. (B) Contact map for Z34C bound to heterodimeric Fc. Lines drawn between Z34C sequence (middle) and sequences from mouse IgG2b C_H2 (top) and C_H3 (bottom) domains indicate interatomic contacts (5 Å cutoff). Red lines indicate contacts that involve only Fc main chain atoms. For comparison, the human IgG1 sequence is shown above and below C_H2 and C_H3 domain sequences, respectively, with dots indicating sequence identity. (C) P307T, Q309L-containing chain of heterodimeric Fc shown in cartoon and colored wheat. Residues P307T, Q309L, and I253 were shown in stick (labeled, underlined). Z34C (magenta) was shown in ribbon with select residues shown in stick, and those within 5 Å of Fc residues I253 and Q309L were labeled. (d) C_H2 domains (ribbon) from chain A (blue) and chain B (cyan) of PBD 2RGS are shown aligned that of the P307T, Q309L chain of mouse IgG2b from the present work. The side chain of N24 (line) from Z34C (pink cartoon) as well as the side chains of residues at positions 309 and 311 (stick) of the C_H2 domains are also shown.

mouse IgG to labeled mouse FcRn results in a luminescence signal. The binding was competed using unlabeled wild-type Ab or different mutant Abs, resulting in a dose-dependent decrease in signal (Fig. 2a). We also measured the relative on- and off-rates of Fc receptor binding by surface bilayer interferometry (Supplementary Fig. 5). At pH 6.0, the mutant mouse IgG2b parental Ab harboring P307T, Q309L on both heavy chain subunits competed as well as wild-type mouse IgG2b for FcRn, indicating that this mutation had no effect on FcRn binding (concentration at half-maximal signal of ~ 0.03 mg/mL) (Fig. 2a). Conversely, the mutant containing I253D on both heavy chain subunits could not compete for FcRn binding up to 2 mg/mL, consistent with previous reports.³³ Interestingly, the mouse BsAb in which one heavy chain subunit contained I253D while the other heavy chain subunit contained P307T, Q309L could compete for FcRn with a half-maximal signal at 0.1 mg/mL. This suggested that while this molecule was impaired for FcRn binding, the activity could be rescued to some extent by having a single functional Fc subunit.

Using surface bilayer interferometry, we confirmed the effects of the mutations on the abilities of the IgG2b variants to bind FcRn (Supplementary Fig. 5a). The results, consistent with those from AlphaScreen, showed the IgG2b I253D parental Ab displayed almost no binding to FcRn. This was also true for IgG2a I253D parental Ab. For IgG2b, the P307T, Q309L parental Ab bound FcRn equally as well as wild-type IgG2b, whereas the analogous mutant in IgG2a displayed somewhat tighter binding to FcRn, having a relative k_{on} ~ 2.7-fold faster

compared to wild-type IgG2a. FcRn binds to the C_H2-C_H3 interface of the Fc, whereas other Fc γ receptors bind to the upper C_H2 region,³⁹ suggesting that the mutations would have little effect on binding. To confirm this, we analyzed the abilities of the mutants to bind mouse Fc γ RI, Fc γ RIIb, Fc γ RIII, and Fc γ RIV. All the mutants displayed on- and off-rates of binding within two-fold of the wild-type antibodies, except in the case of IgG2b binding to Fc γ RI. In this case, the I253D appeared to confer weak binding to the receptor whereas wild-type IgG2b had very low binding to Fc γ RI. The mechanism by which the I253D point mutation conferred slightly enhanced binding to Fc γ RI was unknown, since this mutation had no apparent effect on the ability of IgG2a to bind Fc γ RI. Overall, the mutations had little effect on Fc γ receptor interaction, suggesting that they would have similar effector functions in vivo.

We then examined how in vitro binding to FcRn would manifest with respect to the serum half-life of mouse IgG2b variants. A pharmacokinetic (PK) study was performed to evaluate the effect of the two sets of mutations (I253D or P307T, Q309L) on the serum half-lives of mouse IgG2b and IgG2a Abs harboring the mutation on both heavy chains and on a BsAb harboring one set of mutations on each heavy chain subunit. C57Bl/6 mice were injected intravenously with a single dose of the antibody, and serum levels of each Ab were measured by ELISA over 21 d (Fig. 2B, Table 2, Supplementary Fig. 3C). After ~ 1 h, the clearance rates of all Abs were approximately linear. The I253D parental Ab was cleared from serum rapidly—having a serum half-life of approximately 1.7 d or 0.5 d for the

Table 2. Pharmacokinetics properties of IgG variants.

| | $t_{1/2}^*$ (d) | C_{max}^* ($\mu\text{g}/\text{mL}$) | AUC_{last} ($\text{day}^* \mu\text{g}/\text{mL}$) | AUC_{∞} ($\text{day}^* \mu\text{g}/\text{mL}$) |
|-----------------------------------|--------------------|---|--|--|
| IgG2a variant | | | | |
| anti-human TNF α wild-type | 14.5 \pm 3.4 | 15.8 \pm 4.8 | 104.1 \pm 38.3 | 162.1 \pm 67.5 |
| anti-RSV wild-type | 9.3 \pm 0.7 | 30.8 \pm 3.6 | 87.5 \pm 5.1 | 104.8 \pm 7.7 |
| anti-TNF α I253D | 0.5 \pm 0.1 | 13.8 \pm 8.3 | 10.2 \pm 4.8 | 10.3 \pm 4.8 |
| anti-RSV P307T, Q309L | 12.1 \pm 1.4 | 11.1 \pm 5.3 | 59.3 \pm 12.9 | 82.2 \pm 20.7 |
| anti-TNF α I253D x | 8.8 \pm 1.2 | 26.8 \pm 3.8 | 87.0 \pm 4.2 | 103.4 \pm 4.5 |
| anti-RSV P307T, Q309L | | | | |
| IgG2b variant | | | | |
| anti-human TNF α wild-type | 5.5 \pm 0.3 | 13.6 \pm 7.3 | 98.2 \pm 35.7 | 105.4 \pm 38.1 |
| anti-RSV wild-type | 5.7 \pm 0.9 | 45.6 \pm 40.9 | 137.9 \pm 62.4 | 146.2 \pm 65.5 |
| anti-TNF α I253D | 1.7 \pm 1 | 12.3 \pm 5.9 | 11.6 \pm 3.3 | 11.6 \pm 3.3 |
| anti-RSV P307T, Q309L | 5.4 \pm 0.2 | 23.7 \pm 2.5 | 112.7 \pm 22.9 | 118.9 \pm 24.6 |
| anti-TNF α I253D x | 4.8 \pm 0.2 | 26.1 \pm 5.3 | 90.2 \pm 10.4 | 96.3 \pm 18.5 |
| anti-RSV P307T, Q309L | | | | |

*abbreviations: $t_{1/2}$: elimination half-life, C_{max} : maximum drug concentration, AUC: area under the concentration versus time curve from either point 0 to infinity (AUC_{∞}) or to the last time point with quantifiable concentration (AUC_{last})

IgG2b or IgG2a isotype, respectively. In the case of the IgG2b isotype, the Ab harboring the P307T, Q309L mutations had a serum half-life of 5.4 days, which was similar to that of the two wild-type parental Abs, which had serum half-lives of 5.5 or 5.7 days (Fig. 2B). The BsAb harboring the I253D mutation on one arm and the P307T, Q309L mutations on the other arm, had a half-life of 4.8 days, which was intermediate between the half-lives of its two parental Abs, but was closer to a wild-type half-life than it was to the I253D parental Ab. Analogous to IgG2b Abs, the IgG2a BsAb had a half-life value ($t_{1/2} = 8.8$ d) that was intermediate between that of the two parental Abs (~ 14.5 or 9.3 d), but closer to the wild-type Ab (Supplementary Fig. 3C). This result was consistent with previous observations that antibodies require only a single Fc subunit competent for FcRn binding to retain a long serum half-life.⁴⁰ Consistently, the BsAbs had maximum drug concentration or C_{max} and area under the curve (AUC) values similar to their wild-type parental Abs (Table 2). Together, these results show that mouse IgG2a and IgG2b BsAbs harboring the I253D x P307T, Q309L mutations are suitable for *in vivo* studies, since they have half-life values comparable to that of wild-type Abs. However, they are cleared slightly faster, likely due to having only a single Fc subunit capable of binding FcRn.

Crystal structure of Z34C bound to heterodimeric mouse IgG2b Fc

In an effort to determine the structural basis by which the I253D and P307T, Q309L mutations affected binding to protein A, we determined the crystal structure to 2.7 Å resolution of a heterodimeric Fc harboring the two mutation sets on opposing chains in complex with Z34C,³⁷ a peptide analog of the Z-domain. (Fig. 3, Supplementary Fig. 1a). While Z34C lacked the third helix contained in the canonical Z-domain, it bound mouse IgG2b with similar affinity ($K_D = 2.6 \mu\text{M}$ vs $3.6 \mu\text{M}$) (Supplementary Fig. 6a). Although the peptide was added in greater than two-fold excess of Fc dimer, the asymmetric unit contained a single copy of the heterodimeric Fc

with Z34C bound to only to the chain harboring the P307T, Q309L mutations. The equivalent binding site on the opposite chain was blocked by a symmetry-related Fc molecule (Fig. 3a). The electron density maps confirmed that the subunit bound by Z34C contained the P307T and Q309L mutations (Supplementary Fig. 6b), consistent with the enhanced affinity of these mutants for protein A. The electron densities for the side chain for the I253D mutation as well as the Z34C peptide were also clearly resolved (Supplementary Fig. 6c, d).

The mode of binding of Z34C at the C_{H2} - C_{H3} interface of the P307T, Q309L-containing chain was similar to that observed for its interaction with human IgG1 Fc (PDB 1L6X; Supplementary Fig. 7). Interactions involving the C-terminal helix of Z34C were limited to the C_{H2} domain, whereas the N-terminal helix interacted with both C_{H2} and C_{H3} domains (Fig. 3b). The side chain of P307T adopted a different rotamer than what was observed in the structure of the human IgG1 complex. In the case of the latter, the side chain of T307 formed a hydrogen bond with the side chain of N286 from the C_{H2} domain, which was a threonine in mouse IgG2b (Supplementary Fig. 7b). Neither T307 in the human IgG1 structure nor P307T in the present mouse IgG2b structure were within contact distance of bound Z34C peptide. In the case of the latter, the distance of closest approach was 5.7 Å between P307T atom $C\gamma 2$ and the $N\eta 2$ atom of R31 in Z34C. Similarly, interactions of Q309L with Z34C were limited, with only the $C\delta 1$ atom of Q309L falling within 5 Å of the sidechain of Z34C residue N24 (Fig. 3c). In the P307T, Q309L chain, I253 was positioned on a hydrophobic surface of the Z34C peptide packing between the phenyl ring of F9 and the hydrophobic portion of the R31 sidechain.

P307T and Q309L mutations were not found to result in any large backbone perturbations relative to wild-type mouse IgG2b (PDB 2RGS; Supplementary Fig. 8). Alignment of extended main chain atoms of the C_{H2} domain from the P307T, Q309L-containing chain with the C_{H2} domain from chain A in PDB 2RGS resulted in a positional root mean square deviation (r.m.s.d.) over the same atoms of 0.8 Å. Based on this alignment, the short stretch of sequence from T305 to Q311 encompassing the sites of mutation had an r.m.s.d. of 0.5 Å. The most notable change in structure in the vicinity of the bound peptide relative to wild type mouse IgG2b Fc region (PDB 2RGS) was an altered side chain conformation for Q311 that was required to avoid a clash with Z34C residue N24 (Fig. 3d). The I253D mutation on the opposing Fc chain was also found to result in no significant change in backbone conformation relative to wild-type mouse IgG2b (PDB 2RGS; Supplementary Fig. 8). Alignment of extended main chain atoms of the I253D-containing C_{H2} domain with the C_{H2} domain from chain A in PDB 2RGS resulted in an r.m.s.d. of 0.94 Å, and based on this alignment, for the stretch of sequence from residue V250 to residue T256, an extended main chain r.m.s.d. of 0.8 Å is calculated.

Discussion

Multispecific Abs are an increasingly important part of the biological therapeutic repertoire, but they require more effort than mAbs to produce with high yield and purity. The presence of contaminating Ab fragments or parental Abs in differing concentrations can result in irreproducible functional responses that are required for hit selection and validation. The results of

this work led to a method that can significantly accelerate the production of highly pure mouse BsAbs. We identified two sets of mutations in the C_H2 domain (I253D and P307T, Q309L) that can be incorporated into a set of parental mouse IgG2a or IgG2b molecules for cFAE to allow the formation of mouse BsAb that could be simultaneously purified, re-oxidized, and purified using differential protein A purification from mixed supernatants of parental mAb expression cultures. Conceptually, similar methods exist for human IgG1 BsAbs, wherein one parental Ab contains the H435R, Y436F mutations in the CH3 domain that completely abolish protein A binding.^{34,41} Thus, the formation of a BsAb using the aforementioned construct with the wild-type human IgG1 Ab that binds to protein A with high affinity requires no additional mutations to allow efficient purification of the BsAb. Nonetheless, we have developed a method specifically for mouse IgG2a and IgG2b BsAbs that allows higher throughput purification of the BsAb with little effects on Fc receptor interactions and that should be generally applicable to any mouse Ab subtypes.

One caveat to this method was that the BsAb must be eluted at a pH value just below that at which the molecule was retained on the resin. As a result, greater elution volumes were required to obtain high yields. Nevertheless, the resulting highly pure mouse BsAb molecules retained a serum half-life comparable to wild-type mouse Abs, suggesting that the mutant mouse BsAbs prepared in this way were amenable for *in vivo* studies.

Mouse surrogate models play a critical role in research and development. As a result of their different affinities for Fc γ receptors, mouse IgG isotypes and subtypes vary significantly in their abilities to modulate effector functions such as ADCC and ADCP. Mouse IgG2a and IgG2b with active Fc regions are commonly used for surrogate studies requiring mouse immune cell activity. The mutations introduced here were unlikely to affect these functions because interactions with Fc γ receptors occurred mainly through the regions of the C_H2 domains closest to the hinge region.

While the PK results correlated with *in vitro* FcRn binding results, the extent to which the effects of the I253D mutation could be rescued by pairing with a P307T, Q309L heavy chain subunit was unexpected. In particular, the presence of a single FcRn-binding subunit was sufficient to increase the serum half-life from \sim 1 to 5 days. However, serum half-life can also be influenced by Fab identity,^{42, 43} and indeed the Fab contained in the P307T, Q309L parental may have conferred a modestly extended half-life for IgG2a Abs (Fig. 2b). However, in this example, the effect of Fab identity was less significant than the effects of direct binding site mutations, supporting the suggestion that these bispecific mutants are suitable for *in vivo* studies.

We determined the crystal structure of a heterodimeric mouse IgG2b mutant Fc harboring the I253D mutation in one chain and P307T and Q309L mutations in the other in complex with the protein A analog peptide Z34C. Ten of 15 residues having side chains involved in contacts with the Fc were identical between Z34C and the Z-domain construct used in ITC studies.^{35,44} For two of the five positions that differed from Z-domain, only a single contact involving an atom of the side chain and the Fc was observed. The C β atom of Z34C residue C5 was positioned 4.6 Å from the C γ 2 atom of Fc residue I253, and the C γ 2 of Z34C residue I30 was positioned 4.8 Å from the C γ 1 of the same Fc residue. The side chain of Z34C residue R7,

an asparagine in Z-domain, made contacts with a single residue (N434) in the C_H3 domain. Contacts involving the side chain of M3, a lysine in Z-domain, were similarly limited to N434 and Y436 in the C_H3 domain. The fifth position of difference, R31 in Z34C, was conserved as a lysine in the Z-domain. The residues observed to contribute most significantly to the interaction between Z34C and Fc are identical in Z-domain, consistent with the similar affinity with which Z34C and Z-domain bound to mouse IgG2b. Since crystals of IgG2b in complex with Z-domain diffracted to only 3.9 Å (data not shown), the effects of the I253D and P307T/Q309L sets of mutations were considered in light of the structure of the Fc-Z34C complex.

The structure suggested how the described mutations could alter binding to Z-domain. As previously stated, I253 present in the P307T, Q309L chain of the heterodimeric mIgG2b Fc was observed to pack between the phenyl ring of F9 and the hydrophobic portion of the R31 sidechain. I253 adopted an identical conformation and similarly engaged Z34C in the structure of the human IgG1 complex (Supplementary Fig. 6c). Therefore, the introduction of a negative charge upon mutating this residue to aspartate resulted in reduced affinity by perturbing this hydrophobic interaction. However, the mechanism by which the P307T and Q309L mutations enhanced the affinity for Z-domain could be more complex. These mutations did not significantly perturb the backbone conformation of the C_H2 domain, and direct interactions with Z34C were limited. Furthermore, upon structural alignment of the C_H2 domain of wild-type mouse IgG2b to the P307T, Q309L chain of the present structure, not only should the conformation of Q309 present in structure 2RGS be sterically permitted, but it would also be well-positioned to engage in a hydrogen bond with the side chain of Z34C residue N24. Rather this result could be explained by the observed conformational difference for the Q311 side chain between the wild-type and mutant structures. In one of two chains present in 2RGS, the side chains of Q309 and Q311 were positioned at a distance suitable for a hydrogen bond; in the second chain, χ angles of Q311 were only slightly altered (Fig. 3d). In the structure of the mutant Fc bound to Z34C, the side chain of Q311 was flipped, a change necessary to avoid a clash with Z34C residue N24 (Fig. 3d). Although unlikely to account fully for the near order of magnitude enhancement in affinity for Z-domain of the P307T, Q309L mouse IgG2b mutant relative to wild-type, it was possible that the Q309L mutation facilitated the conformational adjustment of Q311 necessary for Z34C binding by weakening the interaction between the two residues. Also, P307T, Q309L, or both mutations could exert a subtle effect on backbone flexibility that allowed the EF loop to more easily accommodate binding to peptide, an effect that would not be discernible in a static crystal structure of the Fc region bound to the peptide.

Further work will be required to expand this strategy into other species and IgG isotypes and subtypes since the affinity of the wild-type parental mouse Ab for protein A plays a large part in the ease with which a mutant can be separated based on this technique. However, these considerable efforts may be worthwhile due to the large number of BsAbs in development and the routine use of protein A-based resins for their affinity

purification. Likewise, it is possible to use such mutations to prepare bispecific or multispecific Fc fusion molecules.

Materials and methods

Proteins

Mouse IgG2a and IgG2b variants were generated from an anti-human tumor necrosis factor (TNF) mAb (F405L heavy chain subunit molecules) or an anti-respiratory syncytial virus (RSV) mAb (K409R heavy chain subunit molecules). EU numbering of IgG was used throughout this report. Mouse IgG2a and IgG2b heavy chain plasmids were co-transfected with light chain plasmids at a 1:3 molar ratio. Mutations were generated by gene synthesis (Genewiz, Inc.). Proteins were expressed in Expi293 cells (Invitrogen, Inc.) according to the manufacturer's protocol and purified by affinity chromatography using protein G or Ni-NTA resin. BsAbs were produced using the controlled Fab-arm exchange (cFAE) method, according to previously described methods.⁸ Proteins were confirmed by SDS-PAGE and size-exclusion chromatography for purity. The extent of bispecific formation was monitored by analytical HIC using a butyl-NPR column (Tosoh Bioscience LLC). Proteins were eluted using a gradient of 20 mM sodium phosphate pH 6.0 containing 1.5 M to 0 M $(\text{NH}_4)_2\text{SO}_4$ to quantify the relative population of each species. The Z-domain peptide from staphylococcal protein A having the sequence: VDNKFNKEQQNA-FYEILHLPNLNNEEQRNAFIQSLKDDPSQSANLLAEAKKLN-DAQAPK and the Z34C peptide having the sequence: FNMQCQRRFYALHDPNLNNEEQRNAKIKSIRDDC with a disulfide bridge formed between the side chains of C5 and C34 were synthesized (New England Peptide, Inc.) and verified by LC-MS. The concentration of Z-domain was determined using the extinction coefficient at 280 nm of $1490 \text{ M}^{-1} \text{ cm}^{-1}$. All proteins were stored at 4 °C in phosphate-buffered saline pH 7.2 (PBS), unless noted. Z34C used for crystallography was reconstituted from lyophilized powder in 50 mM NaCl, 20 mM HEPES, pH 7.5 and stored at -20°C.

Protein A affinity chromatography

To determine the approximate pH at which each IgG molecule eluted from protein A resin, 1 mg of each sample was loaded onto a mAbSelect SuRe column, composed of immobilized tandem protein A-derived Z-domains (GE Healthcare Life Sciences 11-0034-93) in PBS. Proteins were first eluted using a linear gradient from PBS pH 7.2 to 50 mM citrate pH 3.0 over 30 column volumes. For purification, proteins were eluted in a two-step gradient using 50 mM citrate buffer pH 4.0 and 3.4 for IgG2b and pH 4.9 and 3.4 for IgG2a. Elution fractions were assayed by HIC

Isothermal titration calorimetry

ITC experiments were performed at 25 °C using a MicroCal VP-ITC calorimeter. Both titrant and injectant were dialyzed in PBS. All titrations were performed analogously, having 20 μM IgG in the cell and 200 μM of Z-domain in the syringe. Each 10 μL injection of Z-domain peptide

spanned 20 s, with 5 min spacing between injections. Data were analyzed using Origin software using a 1:1 binding model.

AlphaScreen

Abs were biotinylated using the SureLINK Chromophoric Biotin Labeling kit (KPL Inc.), according to the manufacturer's protocol. His-tagged mouse FcRn was purchased from Sino Biological. Assays were performed in PBS pH 6.0, supplemented with 0.05% (w/v) bovine serum albumin (BSA) and 0.01% (v/v) Tween-20. Note that while BSA can also bind FcRn, this concentration was $\sim 0.0005 \text{ mg/mL}$, which was low compared to the concentration of IgG, and binding between BSA and FcRn is non-competitive with IgG.⁴⁵ Biotinylated wild-type mouse IgG2b at 1 $\mu\text{g/mL}$ was bound to streptavidin-conjugated donor beads, and His-tagged FcRn at 0.2 $\mu\text{g/mL}$ was bound to nickel-conjugated acceptor beads. Competitor Abs were prepared at 2 mg/mL and were serially diluted by 3-fold for each point. Luminescence between 520–620 nm was recorded using an EnVision plate reader (Perkin Elmer). Data were analyzed using Prism 6.01 software (GraphPad Software, Inc.) and fitted using a 4-parameter competition model, as described previously.⁴⁶

Pharmacokinetics studies

Abs were targeted against either anti-respiratory syncytial virus (RSV) F-glycoprotein (P307T, Q309L mutants and parental Abs), or anti-human TNF (I253D mutants and parental Abs) so that there would be no target-mediated internalization, which would confound the PK analysis. The test Abs were injected into C57BL/6 mice intravenously via tail vein at a dose of 10 mg/kg with 6 animals per group. Two sets of animals were used for each test Ab and time points were taken at 30 min, 1 d, 7 d, 21 d and at 1 h, 3 d, 14 d, and 21 d. Serial retro-orbital bleeds were obtained from CO₂-anesthetized mice at the indicated time points and terminal bleeds were taken by cardiac puncture. After 30 min at room temperature, blood samples were centrifuged at 3,000 X g for 15 min and serum collected for analyses. The PK study was approved by the Institutional Animal Care and Use Committee at Janssen Research & Development, LLC. For detection of the mouse test Abs in mouse sera, an electrochemiluminescent immunoassay was used. Streptavidin Gold multi-array 96-well plates (Meso Scale Discovery) were coated for 2 h on a shaker with 50 μL /well of 2 $\mu\text{g/mL}$ of recombinant TNF (R&D systems) for anti-TNF Abs or recombinant RSV-F glycoprotein (Sino Biological) for anti-RSV Abs. Plates were then washed with Tris-buffered saline supplemented with 0.05% (v/v) Tween-20. Serum samples and standards were diluted in 1 X PBS supplemented with 2% (w/v) BSA, 0.5% (v/v) Tween-20, added to plates and incubated for 2 hours on a shaker at room temperature. Bound Ab was detected using a ruthenium-labeled goat anti-mouse IgG, Fc specific (Mesoscale Discovery cat. # R32AC) at 2 $\mu\text{g/mL}$ for 2 h on a shaker. Plates were washed, 200 μL Read Buffer T (Meso Scale Discovery) was added per well, and plates were read on the MSD Sector Imager 6000. Serum concentrations of the Abs were determined from a standard curve using a 5-parameter non-linear regression program in Prism 7 software. For the estimation of terminal Ab half-life, a non-

Table 3. Crystal data, X-ray data, and refinement statistics.

| Crystal data | |
|-------------------------------------|---------------------------------|
| Space group | P ₄ 2 ₁ 2 |
| Complexes per asymmetric unit | 1 |
| Unit cell | |
| a (Å) | 101.5 |
| c (Å) | 135.1 |
| V _m (Å ³ /Da) | 3.07 |
| Solvent content (%) | 59.9 |
| X-ray data | |
| Resolution (Å) | 50.00-2.70 (2.77-2.70)* |
| Measured reflections | 126,458 (9,116) |
| Unique reflections | 19,956 (1,432) |
| Completeness (%) | 99.7 (99.0) |
| Redundancy | 6.3 (6.4) |
| R-merge | 0.053 (0.802) |
| <I/σ> | 21.9 (2.5) |
| Refinement | |
| Resolution (Å) | 38.14-2.70 |
| Number of reflections | 19,947 |
| Number of all atoms | 3,453 |
| Number of waters | 42 |
| R-factor (%) | 20.9 |
| R-free (%) | 25.7 |
| R.M.S.D. | |
| bond lengths (Å) | 0.005 |
| bond angles (°) | 0.858 |
| Mean B-factor (Å ²) | 75.3 |
| Ramachandran | |
| favoured (%) | 98.8 |
| outliers (%) | 0.0 |

*Highest resolution shell is shown in parentheses

compartmental model was used and calculated as: $t_{1/2} = 0.693 / \text{slope}$.⁴⁷ The terminal half-life value for an Ab was determined by taking the average of the $t_{1/2}$ values calculated for each animal within the test group.

Crystallization and structure determination

Z34C peptide was added to recombinant heterodimeric Fc at a 2.2:1 (Fc dimer) molar ratio. Following a 5 h incubation at room temperature, the sample was concentrated to 13.7 mg/mL in buffer containing 50 mM NaCl, 20 mM Tris, pH 8.0. Crystallization experiments employing the sitting drop vapor diffusion method were performed at room temperature using a Mosquito liquid handling robot (TTP Labtech, Ltd). 300 nL drops comprising protein stock and reservoir solution mixed at a 1:1 (v/v) ratio were set up in Corning 3550 plates. Diffraction quality crystals were grown at 20°C and were obtained with a reservoir solution comprising 17% (w/v) PEG 3350, 0.2 M LiCl, 0.1 M Tris, pH 8.0. Crystals were cryo-protected with reservoir solution supplemented with 20% (v/v) glycerol and flash frozen in liquid nitrogen prior to data collection. Diffraction data were collected at the Advanced Photon Source IMCA-CAT beamline 17-ID equipped with a Dectris Pilatus 6M pixel array detector and processed to 2.7 Å with the program XDS.⁴⁸ Initial phases were determined by molecular replacement with the program Phaser⁴⁹ using a crystal structure of mouse IgG2b Fc (PDB ID 2RGS⁵⁰) as a search model. The structure of Z34C from PDB 1L6X³⁸ was subsequently manually docked into available 2Fo-Fc and Fo-Fc electron density followed by additional rounds of rebuilding and refinement using the programs Coot⁵¹ and Phenix,⁵² respectively. Data collection and final refinement statistics are given in Table 3. Analysis of contacts was performed

using the program NCONT as implemented in the CCP4 suite of crystallographic programs⁵³ using a cutoff distance of 5 Å. For comparison to other structures, alignments were performed with either the program LSQMAN⁵⁴ or PyMol (www.schrodinger.com/pymol). Figures were generated with PyMol.

Accession codes

The atomic coordinates and structure factors have been deposited in the Protein Data Bank with accession code 5UBX.

Disclosure of potential conflicts of interest

No potential conflicts of interest were disclosed.

Acknowledgments

We thank Dr. Bernie Scallon (Janssen R&D) for helpful discussions during this work. The authors also acknowledge the staff of the Industrial Macromolecular Crystallography Association Collaborative Access Team (IMCA-CAT) beamline 17-ID at the Advanced Photon Source (APS) of Argonne National Laboratory. We thank Jan Reichert, Aran Labrijn, Janine Schuurman, and Paul Parren for helpful comments to this manuscript.

ORCID

Adam Zwolak  <http://orcid.org/0000-0001-6861-9078>
 Susan H. Tam  <http://orcid.org/0000-0002-4941-8235>
 Dennis R. Goulet  <http://orcid.org/0000-0002-2949-2454>
 Gary L. Gilliland  <http://orcid.org/0000-0001-7394-1846>

References

- Jachimowicz RD, Borchmann S, Rothe A. Multi-specific antibodies for cancer immunotherapy. *BioDrugs: Clinical Immunotherapeutics, Biopharmaceuticals And Gene Therapy*. 2014;28:331-343. doi:10.1007/s40259-014-0091-4. PMID:24638872
- Byrne H, Conroy PJ, Whisstock JC, O'Kennedy RJ. A tale of two specificities: bispecific antibodies for therapeutic and diagnostic applications. *Trends in biotechnology*. 2013;31:621-632. doi:10.1016/j.tibtech.2013.08.007. PMID:24094861
- Thakur A, Lum LG. "NextGen" Biologics: Bispecific Antibodies and Emerging Clinical Results. *Expert opinion on biological therapy*. 2016;16:675-688. doi:10.1517/14712598.2016.1150996. PMID:26848610
- Spieß C, Zhai Q, Carter PJ. Alternative molecular formats and therapeutic applications for bispecific antibodies. *Molecular immunology*. 2015;67:95-106. doi:10.1016/j.molimm.2015.01.003. PMID:25637431
- Weidle UH, Kontermann RE, Brinkmann U. Tumor-antigen-binding bispecific antibodies for cancer treatment. *Seminars in oncology*. 2014;41:653-660. doi:10.1053/j.seminoncol.2014.08.004. PMID:25440609
- Ridgway JB, Presta, LG, Carter, P. 'Knobs-into-holes' engineering of antibody CH3 domains for heavy chain heterodimerization. *Protein Eng*. 1996;9:617-621. doi:10.1093/protein/9.7.617. PMID:8844834
- Gunasekaran K, Pentony M, Shen M, Garrett L, Forte C, Woodward A, Ng SB, Born T, Retter M, Manchulenko K, et al. Enhancing antibody Fc heterodimer formation through electrostatic steering effects: applications to bispecific molecules and monovalent IgG. *J Biol Chem*. 2010;285:19637-19646. doi:10.1074/jbc.M110.117382
- Labrijn AF, Meesters JI, de Goeij BE, van den Bremer ET, Neijssen J, van Kampen MD, Strumane K, Verploegen S, Kundu A, Gramer MJ, et al. Efficient generation of stable bispecific IgG1 by controlled Fab-arm exchange. *Proc Natl Acad Sci U S A*. 2013;110:5145-5150. doi:10.1073/pnas.1220145110. PMID:23479652
- Gramer MJ, van den Bremer ET, van Kampen MD, Kundu A, Kopfmann P, Etter E, Stinehelfer D, Long J, Lannom T, Noordergraaf EH,

- et al. Production of stable bispecific IgG1 by controlled Fab-arm exchange: scalability from bench to large-scale manufacturing by application of standard approaches. *MAbs*. 2013;5:962-973. doi:10.4161/mabs.26233. PMID:23995617
10. Strop P, Ho WH, Boustany LM, Abdiche YN, Lindquist KC, Farias SE, Rickert M, Appah CT, Pascua E, Radcliffe T, et al. Generating bispecific human IgG1 and IgG2 antibodies from any antibody pair. *J Mol Biol*. 2012;420:204-219. doi:10.1016/j.jmb.2012.04.020. PMID:22543237
 11. Schaefer W, Regula JT, Böhner M, Schanzer J, Croasdale R, Dürr H, Gassner C, Georges G, Kettenberger H, Imhof-Jung S, et al. Immunoglobulin domain crossover as a generic approach for the production of bispecific IgG antibodies. *Proc Natl Acad Sci U S A*. 2011;108:11187-11192. doi:10.1073/pnas.1019002108
 12. Lewis SM, Wu X, Pustilnik A, Sereno A, Huang F, Rick HL, Guntas G, Leaver-Fay A, Smith EM, Ho C, et al. Generation of bispecific IgG antibodies by structure-based design of an orthogonal Fab interface. *Nature biotechnology*. 2014;32:191-198. doi:10.1038/nbt.2797
 13. Paul S, Connor J, Nesspor T, Haytko P, Boakye K, Chiu ML, Jiang H. An efficient process of generating bispecific antibodies via controlled Fab-arm exchange using culture supernatants. *Protein Expr Purif*. 2016;121:133-140. doi:10.1016/j.pep.2016.01.014. PMID:26826313
 14. Bruhns P. Properties of mouse and human IgG receptors and their contribution to disease models. *Blood*. 2012;119:5640-5649. doi:10.1182/blood-2012-01-380121
 15. Labrijn AF, Meesters JI, Bunce M, Armstrong AA, Somani S, Nesspor TC, Chiu ML, Altıntaş I, Verploegen S, Schuurman J, et al. Efficient Generation of Bispecific Murine Antibodies for Pre-Clinical Investigations in Syngeneic Rodent Models. *Sci Rep*. 2017;7:2476. doi:10.1038/s41598-017-02823-9
 16. Couch JA, Yu YJ, Zhang Y, Tarrant JM, Fuji RN, Meilandt WJ, Solano H, Tong RK, Hoyte K, Luk W, et al. Addressing safety liabilities of TfR bispecific antibodies that cross the blood-brain barrier. *Sci Transl Med*. 2013;5(183ra157):181-112. PMID:23636093
 17. Lo M, Kim HS, Tong RK, Bainbridge TW, Vernes JM, Zhang Y, Lin YL, Chung S, Dennis MS, Zuchero YJ, et al. Effector-attenuating Substitutions That Maintain Antibody Stability and Reduce Toxicity in Mice. *J Biol Chem*. 2017;292:3900-3908. doi:10.1074/jbc.M116.767749
 18. Nilsson B, Moks T, Jansson B, Abrahamsén L, Elmlblad A, Holmgren E, Henrichson C, Jones TA, Uhlén M. A synthetic IgG-binding domain based on staphylococcal protein A. *Protein Eng*. 1987;1:107-113. doi:10.1093/protein/1.2.107. PMID:3507693
 19. Linhult M, Güllich S, Gräslund T, Simon A, Karlsson M, Sjöberg A, Nord K, Hober S. Improving the tolerance of a protein a analogue to repeated alkaline exposures using a bypass mutagenesis approach. *Proteins*. 2004;55:407-416. doi:10.1002/prot.10616. PMID:15048831
 20. Jansson B, Uhlen M, Nygren, PA. All individual domains of staphylococcal protein A show Fab binding. *FEMS Immunol Med Microbiol*. 1998;20:69-78. doi:10.1016/S0928-8244(97)00108-9. PMID:9514577
 21. Boot JH, Geerts, ME, Aarden LA. Monoclonal anti-peroxidase isotype switch variants. Applications in studies of protein A binding and characterization of rat monoclonal antibodies. *J Immunol Methods*. 1987;103:69-77
 22. Ey PL, Prowse SJ, Jenkin CR. Isolation of pure IgG1, IgG2a and IgG2b immunoglobulins from mouse serum using protein A-sepharose. *Immunochemistry* 1978;15:429-436. doi:10.1016/0161-5890(78)90070-6. PMID:30693
 23. DeLano WL, Ultsch MH, de Vos AM, Wells JA. Convergent solutions to binding at a protein-protein interface. *Science* 2000;287:1279-1283. doi:10.1126/science.287.5456.1279. PMID:10678837
 24. Hinton PR, Xiong JM, Johlfs MG, Tang MT, Keller S, Tsurushita N. An engineered human IgG1 antibody with longer serum half-life. *J Immunol*. 2006;176:346-356. doi:10.4049/jimmunol.176.1.346. PMID:16365427
 25. Dall'Acqua WF1, Woods RM, Ward ES, Palaszynski SR, Patel NK, Brewah YA, Wu H, Kiener PA, Langermann S. Increasing the affinity of a human IgG1 for the neonatal Fc receptor: biological consequences. *J Immunol*. 2002;169:5171-5180
 26. Vaccaro C, Zhou J, Ober RJ, Ward ES. Engineering the Fc region of immunoglobulin G to modulate in vivo antibody levels. *Nature Biotech*. 2005;23:1283-1288. doi:10.1038/nbt1143
 27. Stapleton NM, Andersen JT, Stemerding AM, Bjarnarson SP, Verheul RC, Gerritsen J, Zhao Y, Kleijer M, Sandlie I, de Haas M, et al. Competition for FcRn-mediated transport gives rise to short half-life of human IgG3 and offers therapeutic potential. *Nat Commun*. 2011;2:599. doi:10.1038/ncomms1608
 28. Yeung YA, Leabman MK, Marvin JS, Qiu J, Adams CW, Lien S, Starovasnik MA, Lowman HB. Engineering human IgG1 affinity to human neonatal Fc receptor: impact of affinity improvement on pharmacokinetics in primates. *J Immunol*. 2009;182:7663-7671. doi:10.4049/jimmunol.0804182. PMID:19494290
 29. Hinton PR, Johlfs MG, Xiong JM, Hanestad K, Ong KC, Bullock C, Keller S, Tang MT, Tso JY, Vásquez M, et al. Engineered human IgG antibodies with longer serum half-lives in primates. *J Bio Chem*. 2004;279:6213-6216. doi:10.1074/jbc.C300470200
 30. Roopenian DC, Akilesh, S. FcRn: the neonatal Fc receptor comes of age. *Nat Rev Immuno*. 2007;7:715-725. doi:10.1038/nri2155. PMID:17703228
 31. Junghans RP. Finally! The Brambell receptor (FcRB). Mediator of transmission of immunity and protection from catabolism for IgG. *Immunol Res*. 1997;16:29-57. PMID:9048207
 32. Popov S, Hubbard JG, Kim J, Ober B, Ghete V, Ward ES. The stoichiometry and affinity of the interaction of murine Fc fragments with the MHC class I-related receptor, FcRn. *Mol Immunol*. 1996;33:521-530. doi:10.1016/0161-5890(96)00004-1
 33. Martin WL, West AP, Jr., Gan L, Bjorkman PJ. Crystal structure at 2.8 Å of an FcRn/heterodimeric Fc complex: mechanism of pH-dependent binding. *Mol Cell*. 2001;7:867-877. doi:10.1016/S1097-2765(01)00230-1. PMID:11336709
 34. Tustian AD, Endicott C, Adams B, Mattila J, Bak H. Development of purification processes for fully human bispecific antibodies based upon modification of protein A binding avidity. *MAbs*. 2016;8:828-838. doi:10.1080/19420862.2016.1160192. PMID:26963837
 35. Cedergren L, Andersson R, Jansson B, Uhlen M, Nilsson B. Mutational analysis of the interaction between staphylococcal protein A and human IgG1. *Protein Eng*. 1993;6:441-448. doi:10.1093/protein/6.4.441. PMID:8332602
 36. Braisted AC, Wells, JA. Minimizing a binding domain from protein A. *Proc Natl Acad Sci U S A*. 1996;93:5688-5692. doi:10.1073/pnas.93.12.5688. PMID:8650153
 37. Starovasnik MA, Braisted AC, Wells JA. Structural mimicry of a native protein by a minimized binding domain. *Proc Natl Acad Sci U S A*. 1997;94:10080-10085. doi:10.1073/pnas.94.19.10080. PMID:9294166
 38. Idusogie EE1, Presta LG, Gazzano-Santoro H, Totpal K, Wong PY, Ultsch M, Meng YG, Mulkerrin MG. Mapping of the Clq binding site on rituxan, a chimeric antibody with a human IgG1 Fc. *J Immunol*. 2000;164:4178-4184
 39. Guilliams M, Bruhns P, Saeys Y, Hammad H, Lambrecht BN. The function of Fcγ receptors in dendritic cells and macrophages. *Nat Rev Immunol*. 2014;14:94-108. doi:10.1038/nri3666
 40. Stracke J, Emrich T, Rueger P, Schlothauer T, Kling L, Knaupp A, Hertenberger H, Wolfert A, Spick C, Lau W, et al. A novel approach to investigate the effect of methionine oxidation on pharmacokinetic properties of therapeutic antibodies. *MAbs*. 2014;6:1229-1242. doi:10.4161/mabs.29601. PMID:25517308
 41. Smith EJ, Olson K, Haber LJ, Varghese B, Duramad P, Tustian AD, Oyejide A, Kirshner JR, Canova L, Menon J, et al. A novel, native-format bispecific antibody triggering T-cell killing of B-cells is robustly active in mouse tumor models and cynomolgus monkeys. *Sci Rep*. 2015;5:17943
 42. Igawa T, Tsunoda H, Tachibana T, Maeda A, Mimoto F, Moriyama C, Nanami M, Sekimori Y, Nabuchi Y, Aso Y, et al. Reduced elimination of IgG antibodies by engineering the variable region. *Protein Eng Des Sel: PEDS*. 2010;23:385-392. doi:10.1093/protein/gzq009
 43. Schoch A, Kettenberger H, Mundigl O, Winter G, Engert J, Heinrich J, Emrich T. Charge-mediated influence of the antibody variable domain on FcRn-dependent pharmacokinetics. *Proc Natl Acad Sci U S A*. 2015;112:5997-6002. doi:10.1073/pnas.1408766112
 44. Deisenhofer J. Crystallographic refinement and atomic models of a human Fc fragment and its complex with fragment B of

- protein A from *Staphylococcus aureus* at 2.9- and 2.8-Å resolution. *Biochemistry* 1981;20:2361-2370. doi:10.1021/bi00512a001. PMID:7236608
45. Chaudhury C, Brooks CL, Carter DC, Robinson JM, Anderson CL. Albumin binding to FcRn: distinct from the FcRn-IgG interaction. *Biochemistry*. 2006;45:4983-4990. doi:10.1021/bi052628y. PMID:16605266
46. Vafa O, Gilliland GL, Brezski RJ, Strake B, Wilkinson T, Lacy ER, Scallon B, Teplyakov A, Malia TJ, Strohl WR. An engineered Fc variant of an IgG eliminates all immune effector functions via structural perturbations. *Methods*. 2014;65:114-126. doi:10.1016/j.ymeth.2013.06.035. PMID:23872058
47. Gustafson DL, Bradshaw-Pierce in *Principles of Anticancer Drug Development*. (eds. E. Garrett-Mayer, M. Hidalgo, S.G. Eckhardt & N. J. Clendeninn) (Springer, 2011)
48. Kabsch W. Xds. *Acta crystallographica*. Section D, Biological crystallography. 2010;66:125-132
49. McCoy AJ, Grosse-Kunstleve RW, Adams PD, Winn MD, Storoni LC, Read RJ. Phaser crystallographic software. *J Appl Crystallogr*. 2007;40:658-674. doi:10.1107/S0021889807021206. PMID:19461840
50. Kolenko P, Dohnálek J, Dusková J, Skálová T, Collard R, Hasek J. New insights into intra- and intermolecular interactions of immunoglobulins: crystal structure of mouse IgG2b-Fc at 2.1-Å resolution. *Immunology*. 2009;126:378-385. doi:10.1111/j.1365-2567.2008.02904.x. PMID:18783468
51. Emsley P, Lohkamp B, Scott WG, Cowtan K. Features and development of Coot. *Acta Crystallogr D Biol Crystallogr*. 2010;66:486-501. doi:10.1107/S0907444910007493. PMID:20383002
52. Adams PD, Afonine PV, Bunkóczi G, Chen VB, Davis IW, Echols N, Headd JJ, Hung LW, Kapral GJ, Grosse-Kunstleve RW, et al. PHE-NIX: a comprehensive Python-based system for macromolecular structure solution. *Acta Crystallogr D Biol Crystallogr*. 2010;66:213-221. doi:10.1107/S0907444909052925
53. Winn MD, Ballard CC, Cowtan KD, Dodson EJ, Emsley P, Evans PR, Keegan RM, Krissinel EB, Leslie AG, McCoy A, et al. Overview of the CCP4 suite and current developments. *Acta Crystallogr D Biol Crystallogr*. 2011;67:235-242. doi:10.1107/S0907444910045749
54. Kleywegt GJ. Use of non-crystallographic symmetry in protein structure refinement. *Acta Crystallogr D Biol Crystallogr*. 1996;52:842-857. doi:10.1107/S0907444995016477